JOURNAL OF Materials CHEMISTRY

Analysis of the preparation of In-doped $CaZrO_3$ using a peroxo-oxalate complexation method

Leen van Rij,* Louis Winnubst,† Le Jun‡ and Joop Schoonman

Laboratory for Inorganic Chemistry, Delft University of Technology, Julianalaan 136, 2628 BL, Delft, The Netherlands. E-mail: L.N.vanRij@tnw.tudelft.nl

Received 15th May 2000, Accepted 31st July 2000
First published as an Advance Article on the web 15th September 2000

The wet chemical synthesis of $CaZr_{0.9}In_{0.1}O_{3-\alpha}$ powders *via* a peroxo-oxalate complexation method has been studied in detail using different techniques, *i.e.* TG-DTA, XRD, FT-IR, BET, SEM, EDX, and non-isothermal densification. Using these techniques, the different reaction steps in the calcination process have been clarified. After drying the precipitated complex at 150 °C for 3 h, a mixture of calcium oxalate and an amorphous zirconia phase is found. Between 200 and 450 °C, the calcium oxalate decomposes into calcium carbonate. In the temperature range 450–800 °C, the calcium carbonate decomposes into CaO, while a crystalline zirconia phase appears ($CaZr_4O_9$). In this temperature range, the formation of $CaZrO_3$ is already observed. Further increasing the calcination temperature to 1000 °C leads to a binary mixture of $CaZrO_3$ and $CaIn_2O_4$. When the calcination temperature is increased to around 1500 °C, the $CaIn_2O_4$ phase dissolves into the calcium zirconate to form the desired $CaZr_{0.9}In_{0.1}O_{3-\alpha}$. All compacts sintered at 1550 °C for 10 h show single-phase $CaZr_{0.9}In_{0.1}O_{3-\alpha}$, independent of the calcination temperature. The morphology of the sintered compacts, however, varies with the calcination temperature, due to the presence or absence of a reactive sintering step around 1300 °C. Powders calcined at 1000 °C show a larger grain size in the sintered compact than powders calcined at 1450 or 1550 °C.

1 Introduction

In-doped $CaZrO_3$ belongs to the class of high-temperature perovskite-type proton conductors, like rare earth-doped $BaCeO_3$. Although it has been shown that the conductivity of zirconates is lower than that of cerates,[1–5] In-doped $CaZrO_3$ still shows appreciable protonic conductivity.[6–8] The electrical conductivity of In-doped $CaZrO_3$ has been shown to be purely protonic at temperatures up to 800 °C in the presence of hydrogen gas containing water vapour,[6,8] although in 100% dry hydrogen gas, the electronic conductivity becomes significant at lower temperatures.[9,10] The main advantage of using $CaZrO_3$ is the high chemical and thermal stability of this material[11] with respect to doped $ACeO_3$ (A = Ba, Sr).[11–13] Due to this high stability $CaZrO_3$, is a promising candidate to serve as a solid electrolyte in electrochemical devices, such as solid oxide fuel cells and gas sensors.[9,10,14–17]

Traditionally, the synthesis of $CaZrO_3$ has been carried out through a solid-state reaction. However, it is difficult to obtain very pure and homogeneous powders using a solid-state reaction. Several authors report the existence of an In-rich[7,8,18,19] or Zr-poor phase,[9,10] which is likely to be $CaIn_2O_4$.[7,18,19] Therefore, a wet chemical method was recently developed.[18,19] This method is based on the preparation of an oxalate complex and subsequent calcination to an oxidic perovskite powder. From this process, it is expected that (a) homogeneous mixing of Ca, Zr, and In on an atomic level can be achieved, (b) sub-micron sized particles can be prepared, and (c) densification of the ceramic below 1500 °C in air is feasible. It has been shown that *via* this wet chemical method, a homogeneous powder can be obtained.[19] The synthesis of a powder with sub-micron sized particles suggests the possibility of obtaining a ceramic with a microstructure comprising sub-micron sized grains. Such small grains can influence the electrochemical properties of the electrolyte, as has been demonstrated for $SrCe_{0.95}Yb_{0.05}O_{3-\alpha}$.[20]

In this paper, the different steps in the wet chemical synthesis process, as well as the properties of the obtained powder, such as particle size, sinterability, and composition, will be discussed. TG-DTA, XRD, FT-IR, BET, SEM, EDX, and non-isothermal densification have been used to analyse the products obtained.

2 Experimental

2.1 Sample preparation

The preparation of $CaZrO_3$ powders, doped with 10 mol% of In_2O_3, has been reported in detail previously.[19] The starting materials were indium oxide (99.999% In_2O_3, Aldrich Chem. Co.), calcium carbonate (>99%, Merck), and zirconium oxychloride octahydrate (GR, >99% $ZrOCl_2{\cdot}8H_2O$, E. Merck, Germany). Diammonium oxalate monohydrate (GR, 99.5–101.0% $(NH_4)_2C_2O_4{\cdot}H_2O$, E. Merck, Germany) was used as the complexing agent. Polyethyleneglycol 200 (Merck, pro analyse) was added to the precursor solution as a surfactant (5 wt%). An excess of H_2O_2 (2.5 times the total concentration of metal ions) was also added to this precursor solution. The solution of Ca^{2+}, In^{3+}, and Zr^{4+} (0.1 mol l^{-1}) was added dropwise to a dilute alkaline $(NH_4)_2C_2O_4{\cdot}H_2O$ (>99%, Merck) solution (0.3mol l^{-1}) under constant stirring. To ensure complete complexation, an excess of 25 wt% $(NH_4)_2C_2O_4{\cdot}H_2O$ relative to the total concentration of cations in the precursor solution was used. The complexation was achieved at 45±2 °C and a pH of 9.0±0.05, which was controlled by continuously adding a concentrated NH_4OH solution. The resulting precipitated complex was vacuum-filtered and washed 4 times with 250 ml de-ionized water and 4 times with 250 ml absolute ethanol. Washing with ethanol is assumed to decrease the agglomerate strength and, therefore, to improve the sintering characteristics of the resulting oxide

†Permanent address: University of Twente, Inorganic Materials Science Group, Faculty of Chemical Technology, P.O. Box 217, 7500 AE Enschede, The Netherlands.
‡Permanent address: Department of Inorganic Materials, East China University of Science and Technology, Shanghai 200237, P. R. China.

This journal is © The Royal Society of Chemistry 2000

powder. Calcination of the complex in air was performed in alumina ($T<1000\,^{\circ}C$) or platinum crucibles ($T>1000\,^{\circ}C$). Calcining at temperatures over 1000 °C required that the resulting powder be ground. After calcination, the oxide powders were pressed into pellets with a diameter of 13 mm using cold uniaxial pressing (300 kg cm^{-2}). In order to achieve a better compact after pressing, a binder (Hoechst wachs C micro binder) was added to the mixture (2 wt%).

For comparison, In-doped $CaZrO_3$ was also synthesised *via* the solid-state reaction using $CaCO_3$, ZrO_2, and In_2O_3 powders as precursors.[6] A calculated mixture of the oxides was milled in acetone and subsequently calcined at 1450 °C for 10 h in air. The resulting In-doped $CaZrO_3$ was milled in acetone and pressed into pellets, as described for the solution-derived products.

All compacts were sintered at 1450–1600 °C for 10 h in air using a heating rate of 5 °C min^{-1}.

2.2 Characterisation

In order to identify the different reaction steps in the calcination process, several characterisation experiments were carried out on powders calcined at different temperatures. The precipitated complex and the calcined powders were analysed using scanning electron microscopy (SEM, JEOL LV5800) combined with energy-dispersive X-ray diffraction (EDX, Link EXL II). An indication of the particle sizes of several powders was obtained from these SEM images and from additional BET adsorption measurements. For the analysis of the BET data, it was assumed that the particles were spherical.

The decomposition behaviour of the dried precipitate was studied using temperature-programmed thermogravimetry (TG) and differential thermal analysis (DTA) (ATDBL, M1) up to a temperature of 1050 °C with a heating rate of 10 °C min^{-1}. The complex was heated in a Pt crucible and a couple of Pt–Pt/10%Rh thermocouples was used to register the temperature. The flow rate of the air passed over the sample was 80 ml min^{-1} for the TG analysis and 1 l h^{-1} during DTA. For the DTA analysis, Al_2O_3 powder was used as a reference.

XRD analysis was used to obtain information on the different phases present in the calcined powder at temperatures between 150 and 1550 °C. The experiments were performed using a Philips PW1840 or Brücker D8 advanced diffractometer with Cu-Kα radiation, $\lambda=1.5406$ Å. The JCPDS files were used for the analysis of all XRD data.

The powders calcined in the temperature range between 800 and 1550 °C were studied by Fourier transform infrared spectroscopy (Perkin Elmer FTIR Spectrometer 1000) in the range 4000–400 cm^{-1} in order to identify any amorphous phases that might be present in the calcined powders. The resolution of the FTIR was 4 cm^{-1} and 16 scans were recorded for each spectrum. For the analysis, 0.5–1 mg of powder and 200 mg KBr were thoroughly mixed and then pressed uniaxially at 300 kg cm^{-2} under vacuum for 3 min.

Non-isothermal densification on powders calcined at 1000, 1450, and 1550 °C, respectively, was performed using a Netzsch 410 dilatometer. Isostatically pressed (400 MPa) compacts were heated to 1540 °C at a heating rate of 2 °C min^{-1}. After holding the temperature at 1540 °C for 2 h, the samples were cooled to room temperature at a rate of 4 °C min^{-1}. The density of the sintered compacts was measured using the Archimedes technique with water.

3 Results and discussion

3.1 Formation of the In-doped Ca–Zr oxalate complex

When the Ca^{2+}, Zr^{4+}, and In^{3+}-containing solution is added to the $(NH_4)_2C_2O_4{\cdot}H_2O$–$NH_4OH$ mixture, a white complex is formed. Because the solubility constants of $CaC_2O_4{\cdot}H_2O$, $ZrO(OH)_2$, and $In(OH)_3$ are, respectively, 2.57×10^{-9}, 6.3×10^{-49}, and 6.3×10^{-34}, the yield of the complex is expected to be nearly 100%. The completeness of the complexation reaction is confirmed by the absence of Ca^{2+} in the filtrate, as determined by titration. EDX analysis of the dried complex shows that the Ca : Zr : In ratio in the complex is close to the theoretical value of $CaZr_{0.9}In_{0.1}O_{3-\alpha}$ and uniform throughout the complex.

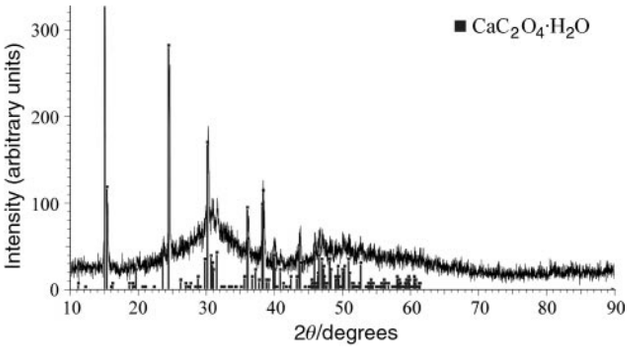

Fig. 1 XRD pattern of the precipitated complex.

Fig. 1 shows the XRD pattern of this complex after drying (150 °C, 2 h). The XRD spectrum can be assigned to $CaC_2O_4{\cdot}H_2O$ (JCPDS 75-1313). The two broad signals around 30 and 50° are attributed to the presence of an amorphous zirconia phase, as found in the synthesis of zirconia.[21] An indium-containing phase cannot be identified from this spectrum. EDX analysis, however, shows the presence of indium.

A scanning electron micrograph of the complex is presented in Fig. 2. As can be seen, a nano-sized powder with an average particle size of about 30 nm has been formed.

3.1.1 Calcination behaviour. The calcination behaviour was studied at temperatures up to 1000 °C using TG and DTA. Using these techniques, it is possible to distinguish the low-temperature reaction steps. XRD analysis and FTIR spectroscopy were used to obtain information on the different phases present in the powder calcined at temperatures between 150 and 1550 °C. SEM images were recorded to obtain information on the morphology of the powders calcined at 1000, 1450, and 1550 °C, as well as to obtain particle sizes. To obtain a more accurate particle size, BET adsorption measurements were performed on the powders calcined at 1000 and 1450 °C.

The results of the TG and DTA experiments are shown in Fig. 3(a) and 3(b), respectively. The first endothermic peak at 165 °C in the DTA curve is due to the evaporation of adsorbed water. The exothermic peaks at 250, 305, 415, and 450 °C are ascribed to the decomposition of the oxalate complexes to carbonates. This decomposition causes a continuous decrease in sample weight in this temperature region due to the release of CO according to reaction 1.

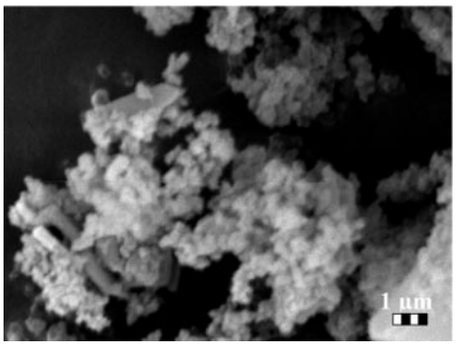

Fig. 2 Scanning electron micrograph of the precipitated complex.

$$C_2O_4^{2-} \rightarrow CO_3^{2-} + CO\uparrow \quad (1)$$

At 660 °C, an endothermic peak is found and attributed to the decomposition of the carbonates to oxides, accompanied by the loss of CO_2, *i.e.* reaction 2.

$$CO_3^{2-} \rightarrow O^{2-}\ (\text{oxide}) + CO_2\uparrow \quad (2)$$

These three regimes have also been reported for oxalate complexation methods used to synthesize barium titanates.[22,23]

The exothermic peak at 550 °C in the DTA curve, as well as the small exothermic peaks at 730, 820, 870, and 935 °C, do not correspond to weight changes in the TG curve. Therefore, these peaks are attributed to solid-state reactions. To further investigate these steps, additional information from different experiments, *i.e.* XRD, is necessary.

The XRD spectra taken after calcining the oxalate complex at 150 (2) (drying), 450 (3), 800 (3), 1000 (3), and 1000 °C (10 h) are presented in Fig. 4.

The peaks observed for the dried complex can all be attributed to $CaC_2O_4{\cdot}H_2O$ (JCPDS 75-1313), as concluded previously. If the complex is calcined at 450 °C, the calcium–oxalate complex decomposes to $CaCO_3$ (JCPDS 772-1214), confirming the conclusions from the TG-DTA experiments. In this powder, as in the dried complex, the broad signals are attributed to an amorphous zirconia phase, as has been found in the synthesis of zirconia.[21] An indium-containing phase could not be identified.

In the powder calcined at 800 °C, three different phases were identified, *i.e.* a $CaZrO_3$ perovskite phase (JCPDS 76-2401), a cubic phase, $Ca_{0.2}Zr_{0.8}O_{1.8}$ (or $CaZr_4O_9$, JCPDS 84-1829), and CaO (JCPDS 78-0649). It is not possible to identify the In-containing phase from the XRD results at 800 °C. The existence of the cubic $CaZr_4O_9$ phase is in accordance with thermodynamic data on undoped $CaZrO_3$. Several authors report the coexistence of a $CaZrO_3$ perovskite and a $CaZr_4O_9$ cubic phase in the CaO–ZrO_2 system at temperatures up to 1300 °C with CaO concentrations between 20 and 50 mol%.[24–28] Ruff *et al.* report the existence of an additional CaO phase when the concentration of CaO in the system is higher than 50 mol%.[29] The observed mixture of different binary oxides confirms the results obtained from the temperature-programmed TG and DTA analysis. Here the exothermic peak at 550 °C and the small exothermic peaks above 720 °C are attributed to solid-state reactions.

If the precipitated powder is calcined at 1000 °C, then the solid-state reactions will progress even further towards formation of the desired In-doped $CaZrO_3$. Fig. 4 shows the XRD pattern obtained after calcining the powder for 3 h at 1000 °C. It can easily be seen that the XRD peaks of the $CaZrO_3$ perovskite phase have increased in intensity. A single-phase material has, however, not been formed yet. Apart from the $CaZrO_3$ phase, three other phases can be identified; the aforementioned CaO and $CaZr_4O_9$ phases and a perovskite $CaIn_2O_4$ phase (JCPDS 17-0643). The intensity of the CaO and $CaZr_4O_9$ peaks, however, has decreased dramatically, indicating a substantial decrease in the amounts of these phases. In other words, the cubic $CaZr_4O_9$ phase reacts with CaO to form stoichiometric $CaZrO_3$ and the unidentified In-containing phase, *e.g.* In_2O_3, reacts with CaO to form $CaIn_2O_4$.

If the complex is calcined at 1000 °C for 10 h, instead of 3 h, the conversion to $CaZrO_3$ and $CaIn_2O_4$ progresses further, to an extent where only these latter two phases can be found.

Fig. 5 shows the XRD results obtained after calcining the powder at 1000 (3), 1000 (10), 1450 (3), and 1550 °C (10 h). For reference, the XRD spectrum of the material obtained in the solid-state reaction at 1450 °C is presented as well.

For the powders calcined at 1450 °C (10 h), the peak intensity ratio of the $CaIn_2O_4$: $CaZrO_3$ peaks increases as compared to the powder calcined at 1000 °C (10 h), indicating

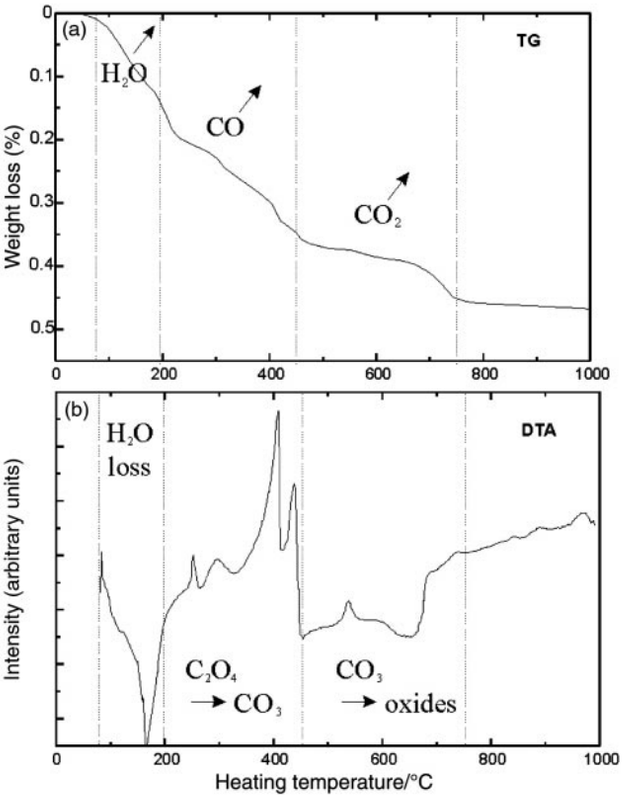

Fig. 3 (a) TG curve of the precipitated complex. (b) DTA curve of the precipitated complex.

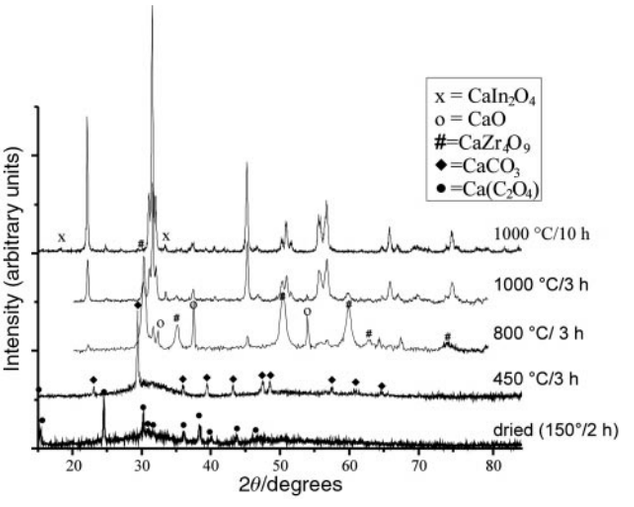

Fig. 4 XRD patterns of the complex calcined at different temperatures between 150 and 1000 °C. The unlabeled peaks are $CaZrO_3$.

that the formation of $CaIn_2O_4$ has progressed further after calcination at this temperature.

Fig. 5 shows that only if the calcination temperature is increased to 1550 °C does the $CaIn_2O_4$ phase dissolve into the $CaZrO_3$ phase to form the desired $CaZr_{0.9}In_{0.1}O_{3-\alpha}$ perovskite. Hence, one high-temperature step ($T \geqslant 1500$ °C) is needed, as opposed to the results obtained by Wei *et al.*,[18] which show that a single phase is found at a temperature of 1000 °C.

From Fig. 5, it can also be concluded that the In-doped powder synthesised *via* a solid-state route consists of two phases, *i.e.* $CaZrO_3$ and $CaIn_2O_4$, in accordance with the wet chemical synthesis route. This result confirms the analysis by other authors.[7,18,19] However, in case of the solid-state reaction route, calcining the material at temperatures above 1500 °C does not result in a single-phase material.[7,9,18,19] In Fig. 6 the

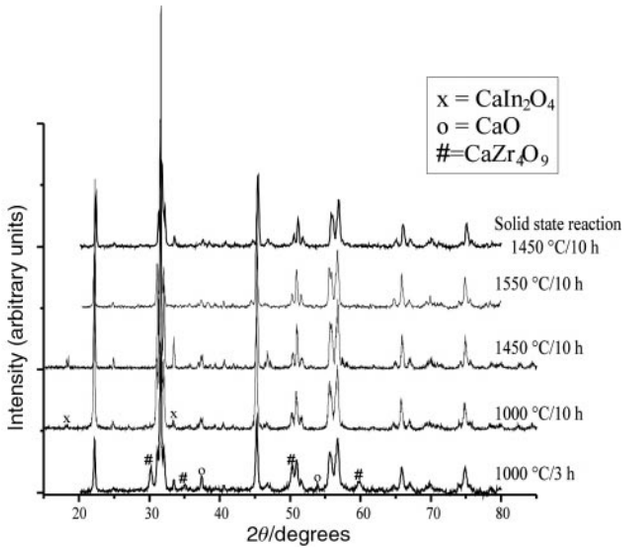

Fig. 5 XRD patterns of the complex calcined at different temperatures between 1000 and 1550 °C, and the XRD pattern of a powder synthesised *via* the solid-state reaction method at 1450 °C for 10 h.

results from the IR measurements on powders calcined at 800, 1000, 1450, and 1550 °C are given. For reference, the IR spectrum of the material obtained from the solid-state reaction conducted at 1450 °C is also presented. The discontinuity at 2300 cm^{-1} is an artifact caused by the spectrometer. The IR spectrum of the powder calcined at 800 °C confirms the existence of $CaZrO_3$ and CaO in the mixture,[30] as observed by XRD. The presence of cubic $CaZr_4O_9$ could not be confirmed, due to the lack of literature data on the IR absorption of this phase. From the IR results, it is obvious that there is still a carbonate phase present at 800 °C. This carbonate phase was not detected by XRD, because it is either amorphous or the fraction of carbonate is too small to be detected by XRD.

At 3440 cm^{-1}, a broad absorption peak appears. Due to the fact that this absorption peak does not disappear at high calcination temperatures (up to 1550 °C), it is assumed that it is caused by protons incorporated into the lattice as hydroxyl groups, and not by a hydroxide phase in the powder. Other authors have reported the presence of an absorption peak around 3400 cm^{-1} for other proton-conducting perovskites, such as $SrZr_{0.95}Y_{0.05}O_{3-\alpha}$,[7] $SrCe_{0.95}Y_{0.05}O_{3-\alpha}$,[2] and $Sr_3(Ca_{0.97}Nb_{0.03})O_{3-\alpha}$.[31]

The morphology of the powders calcined at temperatures of 1000, 1450, and 1550 °C, is presented in Fig. 7. After calcination at 1000 °C, the powder is nano-sized with a particle

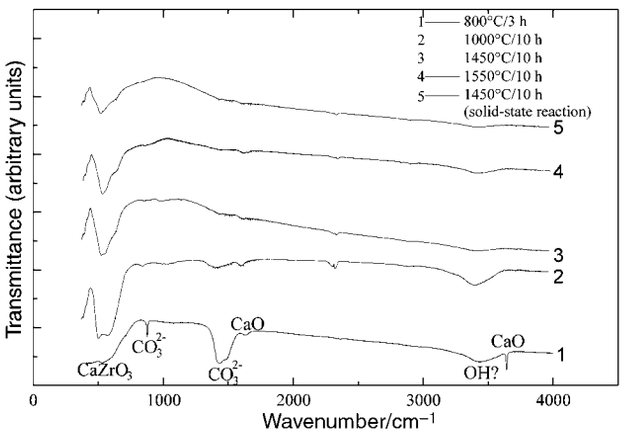

Fig. 6 IR spectra of the complex calcined at different temperatures between 800 and 1550 °C. The IR spectrum for a powder synthesised *via* the solid-state route is added for reference.

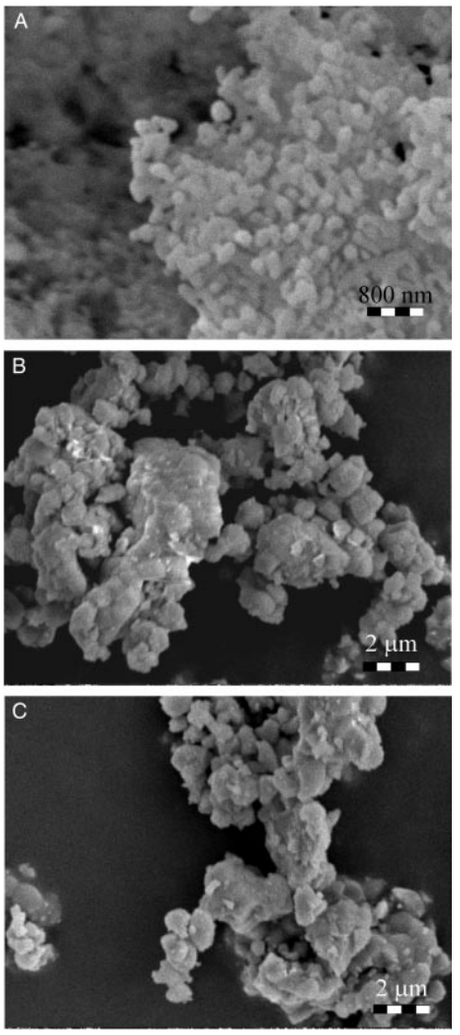

Fig. 7 Scanning electron micrographs of the powders obtained after: (A) calcining for 10 h at 1000 °C; (B) calcining for 10 h at 1450 °C; (C) calcining for 10 h at 1550 °C.

diameter of about 200 nm. These nano-sized particles form, however, large agglomerates with dimensions of several micrometers. Using BET adsorption, a specific surface area of 4.1 $m^2\,g^{-1}$ is obtained, resulting in a calculated average particle size of 400 nm. The elemental ratio in the powder calcined at 1000 °C, *i.e.* Ca : Zr : In, identified using energy-dispersive X-ray diffraction (EDX), is $1 : 0.85 \pm 0.03 : 0.098 \pm 0.002$, *i.e.* close to the theoretical composition.

From Fig. 7, it can be seen that, after calcining the powder at 1450 °C, the particle size increases to about 1–2 μm. BET adsorption measurements show that the average particle diameter increases to 3.1 μm. From the SEM image, it is obvious that further increase of the calcination temperature to 1550 °C does not result in an increase in particle size.

3.2 Sintering behaviour

Fig. 8 presents the morphology of pellets sintered at 1550 °C for 10 h, using powders calcined at 1000 (3 h), 1450, and 1550 °C. As can be seen, the average grain size in the sintered compact from material with a calcination temperature of 1000 °C (1–2 μm) is much larger than those of the powders calcined at 1450 or 1550 °C (0.4–0.7 μm). The reason for this is not obvious. To be able to better understand the sintering behaviour of the powder, further experiments were performed. In particular, non-isothermal densification was studied, and the results are shown in Fig. 9(a). This shows the densification

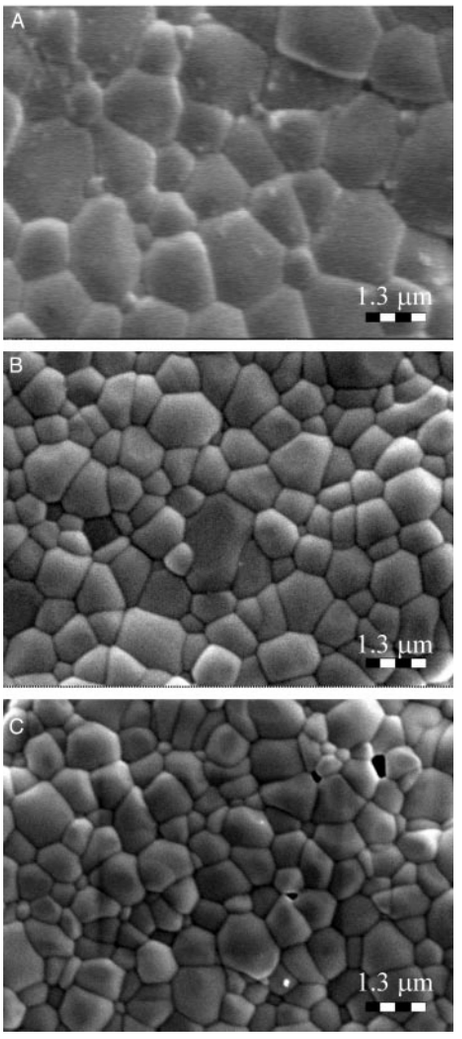

Fig. 8 SEM micrographs of sintered $CaZr_{0.9}In_{0.1}O_{3-\alpha}$ compacts. (A) After calcination at 1000 °C for 3 h and sintering at 1550 °C for 10 h. (B) After calcination at 1450 °C for 3 h and sintering at 1550 °C for 10 h. (C) After calcination at 1550 °C for 3 h and sintering at 1550 °C for 10 h.

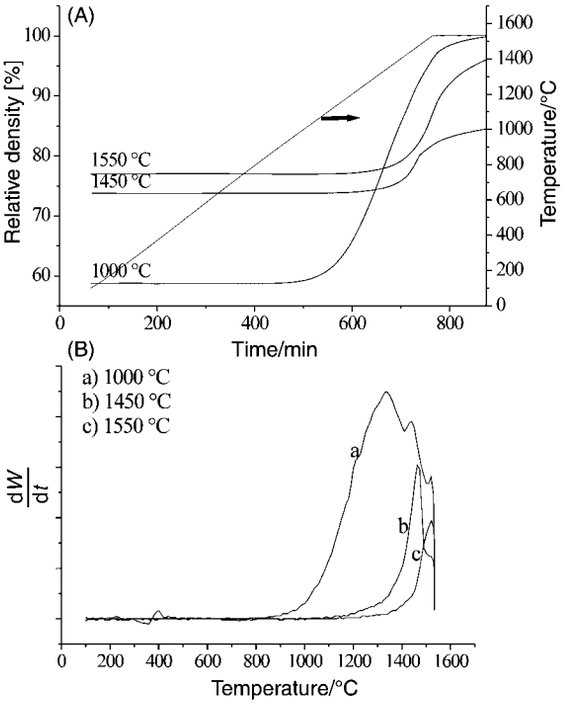

Fig. 9 (A) Densification curves of powders calcined at 1000 (3 h), 1450, and 1550 °C. (B) Derivatives of the densification curves for powders calcined at 1000, 1450, and 1550 °C.

Table 1 Densities of the green and final compacts and temperatures where sintering starts and the maximum sinter speed occurs

Calcination temperature/ °C	Green density (%)	Final density (%)	Point at which sintering starts/ °C	Temperature of maximum sinter speed/ °C
1000	54	93	*ca.* 1000	1310
1450	74	85	*ca.* 1100	1460
1550	78	87	*ca.* 1350	1590

curves of green compacts made from powders calcined at 1000 (3 h), 1450, and 1550 °C. Fig. 9(b) shows the derivatives of these curves. In Table 1, the temperatures of the maximum sinter speed are presented, along with the green and final densities of these powders. It should be noted that the complex calcined at 1000 °C shows three maxima in the sintering speed, *i.e.* at 1335, 1440, and 1515 °C. Also, the powder calcined at 1450 °C shows more than one maximum (1465 and 1520 °C). It is remarkable that the latter two maxima for the powder calcined at 1000 °C coincide with the maxima found for the powders calcined at 1450 and 1550 °C. The same holds for the behaviour of the powder calcined at 1450 °C, where the second maximum is found at the same temperature as the maximum for the powder calcined at 1550 °C. This behaviour can be explained according to the findings of the powder synthesis, as described earlier. Upon calcining the complex at different temperatures, it was found that a single phase is only formed after calcination at 1550 °C.

When the powder calcined at 1000 °C is sintered, reactive sintering takes place and the four oxides react to form the perovskite phases ($CaIn_2O_4$ and $CaZrO_3$), as discussed above. According to the densification experiment, this happens in a broad temperature range with a maximum at 1335 °C. This reaction leads to sintering of the sample and, probably, to a large increase in grain size (see also Fig. 8). Around 1450 °C, $CaZr_{0.9}In_{0.1}O_{3-\alpha}$ (the second maximum in the densification of the powder calcined at 1000 °C) is formed from the two perovskites, associated with an increase in the density of the sample. The last maximum, found at 1520 °C, is the temperature at which the $CaZr_{0.9}In_{0.1}O_{3-\alpha}$ phase exhibits a maximum sintering speed. This analysis leads to the conclusion that, in order to obtain a single-phase perovskite $CaZr_{0.9}In_{0.1}O_{3-\alpha}$, one temperature step of 1500 °C is needed. This conlusion is confirmed by the XRD analysis of the sintered compacts made from powders calcined at 800, 1450, and 1550 °C, shown in Fig. 10. As can be seen, all the sintered pellets are single-phase $CaZr_{0.9}In_{0.1}O_{3-\alpha}$. Hence, the calcination temperature of the powders does not have an effect on the final crystal structure of the material, as long as the material is sintered at a temperature greater than 1500 °C.

However, it should be stressed again that the calcination temperature does have an effect on the final grain size in the sintered compact. This result suggests that the grain size can be controlled in the final compact. The possibility of controlling the grain size in the final compact will be important for the optimization of the electrical conductivity of this material. In the case of predominant bulk conductivity, calcination of a powder at 1000 °C for 3 h and subsequent sintering at 1550 °C leads to a higher electrical conductivity, while in the case of predominant grain boundary conductivity, a calcination temperature of 1550 °C would be favourable. The influence of the microstructure on the electrochemical properties of $CaZr_{0.9}In_{0.1}O_{3-\alpha}$ is currently being investigated.

Fig. 11 shows the relative density of compacted $CaZr_{0.9}In_{0.1}$-

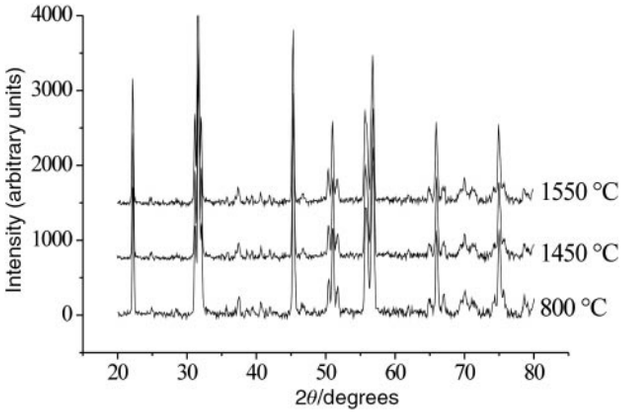

Fig. 10 Comparsion of XRD patterns of sintered compacts [1550 °C (10 h)] for different calcination temperatures.

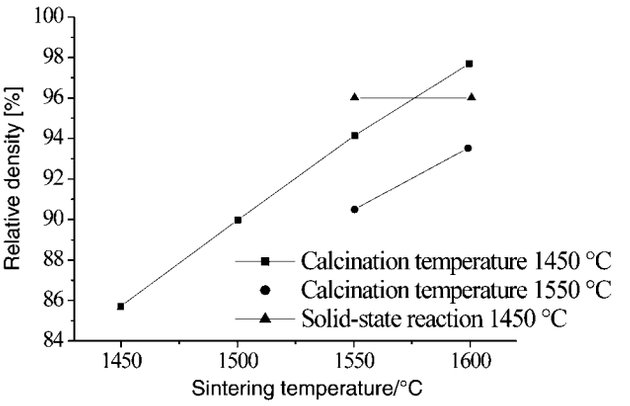

Fig. 11 Relative density of $CaZr_{0.9}In_{0.1}O_{3-\alpha}$ compacts as a function of sintering temperature.

$O_{3-\alpha}$ pellets sintered for 10 h at different temperatures. The effect of sintering temperature is given for wet chemically synthesized powders calcined at 1450 and 1550 °C, and for a powder synthesised *via* the solid-state route. From Fig. 11, it is apparent that the density of the sintered pellet increases with sintering temperature for the wet chemically synthesised powder. It can also be seen from this figure that a sintering temperature of 1550 °C, or higher, is needed to form a dense ceramic (>90%). This could also explain the low densities found after the dilatometer experiments, as shown in Fig. 9(a), with a maximum temperature of 1540 °C.

4 Conclusions

In-doped $CaZrO_3$ has been synthesized *via* a peroxo-oxalate complexation method. In the calcination process, different steps are identified. After drying the precipitated complex at 150 °C, calcium oxalate and an amorphous cubic zirconium oxide phase are found. Calcining the material at 450 °C leads to decomposition of the oxalate into calcium carbonate, while the amorphous zirconia phase is still present. At a calcination temperature of 800 °C the amorphous zirconium phase reacts with $CaCO_3$ to form cubic $CaZr_4O_9$, perovskite $CaZrO_3$, and CaO. Further increase of the calcination temperature leads to a binary mixture of perovskite phases $CaIn_2O_4$ and $CaZrO_3$. Finally, if the calcination temperature is increased to 1500 °C or higher, the desired solid solution, $CaZr_{0.9}In_{0.1}O_{3-\alpha}$, is formed.

Hence, the reaction scheme can be given as follows:

$$\text{Precipitated complex} \xrightarrow{150\ ^\circ\text{C}} \text{Ca}(\text{C}_2\text{O}_4) + \text{Amorphous zirconia}$$

$$\xrightarrow{450\ ^\circ\text{C}} \text{CaCO}_3 + \text{Amorphous zirconia}$$

$$\xrightarrow{800\ ^\circ\text{C}} \text{CaO} + \text{CaZr}_4\text{O}_9 + \text{CaZrO}_3$$

$$\xrightarrow{1000\ ^\circ\text{C}/3\ \text{h}} \text{CaIn}_2\text{O}_4 + \text{CaO} + \text{CaZr}_4\text{O}_9 + \text{CaZrO}_3$$

$$\xrightarrow{1000\ ^\circ\text{C}/10\ \text{h}} \text{CaIn}_2\text{O}_4 + \text{CaZrO}_3$$

$$\xrightarrow{1500\ ^\circ\text{C}} \text{CaZr}_{0.9}\text{In}_{0.1}\text{O}_{3-\alpha}$$

It has been found that varying the calcination temperature leads to different sintering behaviour for the compacted pellets, due to the presence of different phases in the materials. If the compact is sintered at a temperature of 1500 °C or more, single phase $CaZr_{0.9}In_{0.1}O_{3-\alpha}$ is always formed. The grain size of the densified material, however, can be influenced by the calcination temperature. Powder calcined at 1000 °C leads to a densified material with a grain size of 1–2 μm, while a calcination temperature of 1450 or 1550 °C leads to a grain size of 0.4–0.7 μm.

Acknowledgements

The authors would like to thank Dr T. P. Raming and Dr ir. B. Kerkwijk from the University of Twente for carrying out the dilatometer experiments. Ing. R. C. van Landschoot, Delft University of Technology, is acknowledged for fruitful discussions and useful experimental assistance. One of the authors, J. Le, is grateful to the China Scholarship Council for financial support. He thanks Prof. J. Schoonman for his hospitality.

References

1 H. Iwahara, *Solid State Ionics*, 1995, **77**, 289.
2 H. Iwahara, *Solid State Ionics*, 1996, **86–88**, 9.
3 H. Iwahara, *Solid State Ionics: Materials and Applications*, 1992, 247.
4 R. A. De Souza, J. A. Kilner and C. Jeynes, *Solid State Ionics*, 1997, **97**, 409.
5 N. Matsunami, T. Shimura and H. Iwahara, *Solid State Ionics*, 1998, **106**, 155.
6 T. Yajima, H. Kazeoka and H. Iwahara, *Solid State Ionics*, 1991, **47**, 271.
7 H. Iwahara, T. Yajima, T. Hibino, K. Ozaki and H. Suzuki, *Solid State Ionics*, 1993, **61**, 65.
8 N. Kurita, N. Fukatsu, K. Ito and T. Ohashi, *J. Electrochem. Soc.*, 1995, **142**, 1552.
9 W. Engelen, A. Buekenhoudt, J. Luyten and F. DeSchutter, *Solid State Ionics*, 1997, **96**, 55.
10 M. Makri, A. Buekenhoudt, J. Luyten and C. G. Vayenas, *Ionics*, 1996, **2**, 282.
11 K. D. Kreuer, *Solid State Ionics*, 1997, **97**, 1.
12 S. V. Bhide and A. V. Virkar, *J. Electrochem. Soc.*, 1999, **146**, 2038.
13 M. J. Scholten, J. Schoonman, J. C. v. Miltenburg and H. A. J. Oonk, *Solid State Ionics*, 1993, **61**, 83.
14 N. Kurita, N. Fukatsu and T. Ohashi, *J. Jpn. Inst. Met.*, 1994, **58**, 782.
15 N. Fukatsu, N. Kurita, E. A. Koltypin and T. Ohashi, *Solid State Ionics*, 1998, **113-115**, 219.
16 N. Kurita, K. Otsuka, N. Fukatsu and T. Ohashi, *Solid State Ionics*, 1995, **79**, 358.
17 T. Yajima, K. Koide, N. Fukatsu, T. Ohashi and H. Iwahara, *Sens. Actuators, B*, 1993, **13–14**, 697.
18 W. Yang, G. Li and Z. Sui, *J. Mater. Sci. Lett.*, 1998, **17**, 241.

19 J. Le, L. N. van Rij, R. C. Van Landschoot and J. Schoonman, *J. Eur. Ceram. Soc.*, 1999, **19**, 2589.
20 I. Kosacki and H. U. Anderson, *Solid State Ionics*, 1998, **97**, 429.
21 G. T. Mammot, P. Barnes, S. E. Tarling, S. L. Jones and C. J. Orman, *J. Mater. Sci.*, 1991, **26**, 4054.
22 S. van der Gijp, A. J. A. Winnubst and H. Verweij, *J. Mater. Chem.*, 1998, **8**, 1251.
23 S. Suasmoro, S. Pratapa, D. Hartanto, D. Setyoko and U. M. Dani, *J. Eur. Ceram. Soc.*, 2000, **20**, 309.
24 J. R. Hellmann and V. S. Stubican, *J. Am. Ceram. Soc.*, 1983, **66**, 260.
25 V. S. Stubican and J. R. Hellmann, *Mater. Sci. Monogr.*, 1982, **10**, 257.
26 T. Nishino, *Nippon Kagaku Kaishi*, 1981, **10**, 1681.
27 R. C. Garvie, *J. Am. Ceram. Soc.*, 1968, **51**, 553.
28 V. S. Stubican and S. P. Ray, *J. Am. Ceram. Soc.*, 1977, **60**, 534.
29 O. Ruff, F. Ebert and E. Stephan, *Z. Anorg. Allg. Chem.*, 1929, **180**, 215.
30 R. A. Nyquist and R. O. Kagel, *Infrared spectra of inorganic compounds*, Academic Press, New York and London, 1971.
31 A. S. Nowick and D. Yang, *Solid State Ionics*, 1995, **77**, 137.